Endoplasmic reticulum–to–Golgi trafficking of procollagen III via conventional vesicular and tubular carriers

Yukihiro Hirata[a], Yuto Matsui[a], Ikuo Wada[b], and Nobuko Hosokawa[a,*]
[a]Laboratory of Molecular and Cellular Biology, Institute for Frontier Life and Medical Sciences, Kyoto University, Kyoto 606-8507, Japan; [b]Department of Cell Science, Institute of Biomedical Sciences, Fukushima Medical University School of Medicine, Fukushima 960-1295, Japan

ABSTRACT **Collagen is the major protein component of the extracellular matrix. Synthesis of procollagens starts in the endoplasmic reticulum (ER), and three α chains form a rigid triple helix 300–400 nm in length. It remains unclear how such a large cargo is transported from the ER to the Golgi apparatus. In this study, to elucidate the intracellular transport of fibril-forming collagens, we fused cysteine-free GFP to the N-telopeptide region of procollagen III (GFP-COL3A1) and analyzed transport by live-cell imaging. We found that the maturation dynamics of procollagen III was largely different from that of network-forming procollagen IV. Proline hydroxylation of procollagen III uniquely triggered the formation of intralumenal droplet-like structures, similarly to events caused by liquid–liquid phase separation, and ER exit sites surrounded large droplets containing chaperones. Procollagen III was transported to the Golgi apparatus via vesicular and tubular carriers containing ERGIC53 and RAB1B; this process required TANGO1 and CUL3, which we previously reported to be dispensable for procollagen IV. GFP-COL3A1 and mCherry-α1AT were cotransported in the same vesicle. Based on these findings, we propose that shortly after ER exit, enlarged carriers containing procollagen III fuse to ERGIC for transport to the Golgi apparatus by conventional cargo carriers.**

Monitoring Editor
Elizabeth Miller
MRC Laboratory of Molecular Biology

Received: Jul 30, 2021
Revised: Dec 17, 2021
Accepted: Dec 23, 2021

INTRODUCTION

Collagens are the major components of extracellular matrix (ECM) proteins in animals, and 28 types of collagens are encoded in the human genome (Gordon and Hahn, 2010; Ricard-Blum, 2011; Mouw *et al.*, 2014; Bella, 2016). Typical fibril-forming collagens (types I, II, III, and V) constitute long fibers in the ECM to support the tissues and organs, and network-forming collagens such as type IV create lattice structures to generate basement membranes. Three α chains of collagens synthesized in the endoplasmic reticulum (ER) form a triple helix starting at the C-terminus, nucleated by the association of the C-propeptides (Myllyharju and Kivirikko, 2004; Canty and Kadler, 2005). After undergoing protein modifications, including proline hydroxylation, disulfide bond formation, and glycosylation, the procollagen molecules acquire the correct conformation, exit the ER, and are delivered to the late secretory apparatus for exocytosis.

Secretory proteins synthesized in the ER are exported from the ER exit site (ERES) via COPII vesicles with a diameter of 60–80 nm (Barlowe *et al.*, 1994; Lee *et al.*, 2004; Zanetti *et al.*, 2011; Brandizzi and Barlowe, 2013; Aridor, 2018). However, procollagen trimers assembled in the ER are rigid and 300–400 nm in length (Bachinger *et al.*, 1982), a size that cannot be accommodated by conventional COPII vesicles (Fromme and Schekman, 2005; Malhotra and Erlmann, 2015). One proposed mechanism for generating larger COPII vesicles involves the function of the CUL3–KLHL12 ubiquitin–ligase complex, which enlarges COPII vesicles by monoubiquitinating the Sec31 coat protein (Jin *et al.*, 2012). Since the discovery that TANGO1 is required for the ER exit of collagen VII (Saito *et al.*, 2009), the mechanisms by which large cargos such as collagens are

This article was published online ahead of print in MBoC in Press (http://www.molbiolcell.org/cgi/doi/10.1091/mbc.E21-07-0372) on January 19, 2022.

*Address correspondence to: Nobuko Hosokawa (nobukoh@infront.kyoto-u.ac.jp).

Abbreviations used: α1AT, α_1-antitrypsin; CHX, cycloheximide; COPII, coat protein complex II; ER, endoplasmic reticulum; ERES, ER exit site; ERGIC, ER–Golgi intermediate compartment; SFM, serum-free medium; siRNA, small interfering RNA.

exported from the ER have been extensively analyzed (Raote and Malhotra, 2021). TANGO1 and cTAGE5, another MIA/TANGO1 family protein, interact with the Sec23 inner coat protein (Saito *et al.,* 2011), which delays the association of the Sec31 outer coat protein, resulting in the formation of large tubular carriers (Ma and Goldberg, 2016). Alternatively, TANGO1 assembles into a ring structure at the ERES (Raote *et al.,* 2017), and the large carriers containing collagens are generated by incorporating ERGIC membranes (Santos *et al.,* 2015). Recently, intracellular transport of procollagen I was analyzed using live-cell imaging, revealing that procollagens are transferred from the juxtanuclear ER to the Golgi without using vesicles for transport (McCaughey *et al.,* 2018). These findings led to the development of the "short-loop pathway" model, which entails a tunneling mechanism between the ER and Golgi (McCaughey and Stephens, 2019; Raote and Malhotra, 2019, 2021).

We recently analyzed the intracellular transport of GFP-tagged procollagen IV, a network-forming collagen that constitutes the major component of the basement membranes, and found that procollagen IV is transported by vesicles ~400 nm in diameter (Matsui *et al.,* 2020). These vesicles are similar in size to the carrier of conventional cargo but do not contain the ERGIC membrane, suggesting that procollagen IV uses an ER-to-Golgi transport pathway distinct from that of conventional cargo.

In this study, to elucidate the mechanism underlying intracellular transport of fibril-forming collagens, we introduced cysteine-free SGFP2 (cfSGFP2; Suzuki *et al.,* 2012) into the N-telopeptide region of procollagen III, allowing us to detect the GFP signal after secretion and cleavage of the N-propeptide by procollagen N-proteinase. We found that procollagen III was transported from the ER to the Golgi apparatus via tubulo-vesicular structures that contain the ERGIC membrane. In addition, we found that procollagen III was condensed into large droplets similar to those formed by liquid–liquid phase separation before exit from the ER. We also analyzed the factors required for procollagen export from the ER and found that factors including SAR1, TANGO1, and CUL3 were necessary for the export of procollagen III.

RESULTS

GFP-COL3A1 is secreted and remodeled in the extracellular matrix

To analyze ER-to-Golgi transport of procollagen III in live cells, we introduced cfSGFP2 into the N-telopeptide region of COL3A1 (GFP-COL3A1; Figure 1A). Procollagen III consists of a homotrimer of three α1(III) chains (COL3A1). We predicted that the fluorescent tag in the N-telopeptide would not inhibit formation of the triple helix of procollagen III, as collagens form trimers in the ER starting from the C-terminus. In addition, we anticipated that GFP-COL3A1 would be detected after secretion, when the N-propeptides were cleaved. When cells were cultured in the absence of ascorbate, procollagens were retained in the ER due to the hypohydroxylation of Pro residues (Beck *et al.,* 1996). GFP-COL3A1 expressed in COS-7 cells was distributed in a fine reticular network colocalized with PDI-mCherry, an ER marker, confirming that GFP-COL3A1 was synthesized and accumulated in the ER in the absence of ascorbate (Figure 1B). Within 1 h after addition of ascorbate, GFP-COL3A1 became concentrated in the perinuclear region, where PDI-mCherry was excluded (Supplemental Figure S1, A and B). Coexpression of GFP-COL3A1 and Golgi-BFP, a cis-Golgi marker, confirmed that this region was the Golgi apparatus (Figure 1C). GFP-COL3A1 moved to the cis-Golgi ~30 min after the addition of ascorbate and subsequently disappeared from the Golgi region, indicating that GFP-COL3A1 was transported to the late secretory pathway (Figure 1D and Movie 1).

We next expressed GFP-COL3A1 in COS-7 and the human rhabdomyosarcoma cell line RD, which produces collagen III (Krieg *et al.,* 1979), and cultured the cells in the presence of ascorbate. Fibrillar GFP signals lining the cells were detected by live-cell imaging (Figure 1E) and immunostaining (Supplemental Figure S2, A and B) in both cell lines, indicating that GFP-COL3A1 accumulated in the ECM. GFP fibrils were detected without permeabilization of the fixed cells (Supplemental Figure S2A), and HSP47, an ER marker, did not colocalize with these fibrils even after cell permeabilization (Supplemental Figure S2A), confirming that GFP-COL3A1 was secreted and deposited in the ECM. Because the cleavage of N-propeptide from procollagen III is slow and less efficient than cleavage of the peptide from procollagens I and II (Hulmes 2002), extracellular collagen III fibers are also stained by an antibody that recognizes the N-propeptide of procollagen III. GFP-COL3A1 fibrils were detected within the long endogenous collagen III fibers in RD cells (Supplemental Figure S2B). Interestingly, extracellular GFP-COL3A1 fibers were dynamically remodeled in RD cells (Supplemental Figure S2C). Pulse-chase analysis confirmed that only GFP-COL3A1 trimers were secreted into the culture media (Supplemental Figure S3A). Trimers containing GFP-COL3A1 were detected as triplet bands when electrophoresed under nonreducing conditions (Supplemental Figure S3A), suggesting that procollagen III trimers containing one to three GFP-COL3A1 chains were generated in RD cells. The level of GFP-COL3A1 expression was 9.2 ± 0.97% of that of endogenous procollagen III (Supplemental Figure S3B, $n = 8$), and GFP-COL3A1 was secreted into the medium with kinetics similar to those of endogenous procollagen III (Supplemental Figure S3C). Taken together, these observations indicate that GFP-COL3A1 is synthesized and secreted as a trimer to form fibrils similar to endogenous type III collagen.

GFP-COL3A1 is transported by vesicles from the endoplasmic reticulum to the Golgi apparatus

To elucidate how procollagen III is transported from the ER to the Golgi apparatus, we expressed GFP-COL3A1 and PDI-mCherry in RD cells and analyzed the transfectants by confocal microscopy. GFP-COL3A1–containing vesicles that lacked PDI-mCherry moved to the Golgi apparatus after addition of ascorbate (Figure 2A and Supplemental Movie 2), whereas few GFP-COL3A1–containing vesicles were observed in the absence of ascorbate, which was quantified by counting particles that did not colocalize with PDI-mCherry using the ComDet plugin of ImageJ (Figure 2B).

To compare vesicles containing GFP-COL3A1 with those carrying conventional cargos, we transfected GFP-α1AT into RD cells. Vesicles carrying GFP-α1AT moved from the ER to the Golgi apparatus similarly to those containing GFP-COL3A1 (Supplemental Figure S4 and Supplemental Movie 3). The diameters of both kinds of vesicles were 350–400 nm (Figure 2C). Together, these data indicate that GFP-COL3A1 is transported from the ER to the Golgi apparatus in vesicles 350–400 nm in diameter that are similar to those carrying the conventional model cargo GFP-α1AT.

GFP-COL3A1 is transported by vesicular and tubular carriers containing RAB1 and ERGIC53

To characterize the transport vesicles carrying procollagen III, we expressed GFP-COL3A1 or GFP-α1AT and mScarlet-RAB1B into RD cells. RAB1 localizes in transport vesicles and regulates the ER-to-Golgi trafficking of conventional cargo (Plutner *et al.*, 1991; Saraste *et al.*, 1995). As expected, GFP-α1AT–containing vesicles

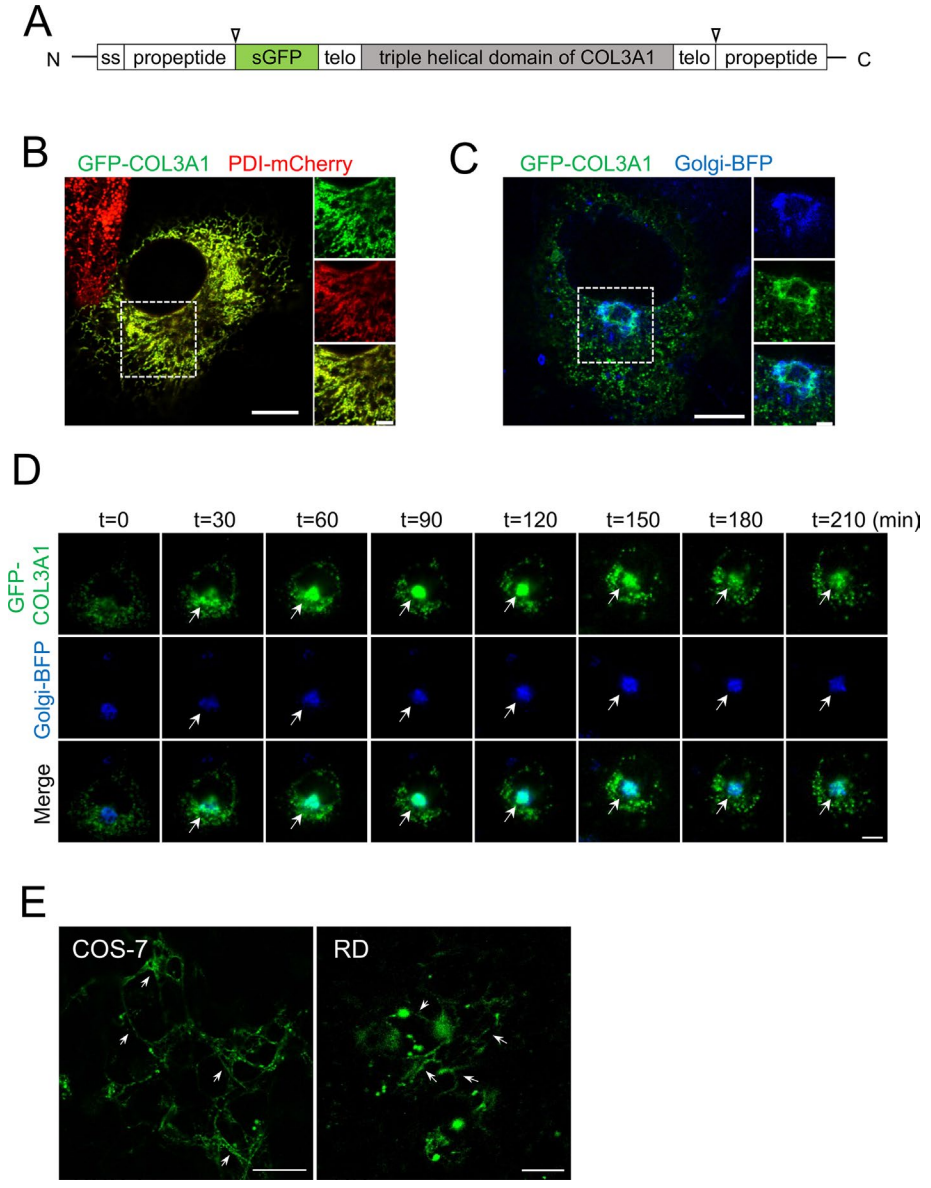

FIGURE 1: GFP-COL3A1 is secreted from the ER via the Golgi apparatus to the extracellular space, where it forms fibrils. (A) Schematic of the GFP-COL3A1 construct. Cysteine-free SGFP2 was inserted into the N-telopeptide of human COL3A1. N- and C-propeptide cleavage sites are indicated by the arrowheads. ss, signal peptide; sGFP, cysteine-free SGFP2; telo, telopeptide. (B) Live-cell imaging of COS-7 cells transiently expressing GFP-COL3A1 (green) and PDI-mCherry (red) in the absence of ascorbate. Right panels show images in each channel (green, red, and merge) of the region indicated by the white box. Scale bars, 10 μm (left panel) and 3 μm (right panels). (C) Same as in B except that the cells were transiently transfected with GFP-COL3A1 (green) and Golgi-BFP (blue) and treated with ascorbate for 1 h. Image of each channel (blue, green, and merge) of the white-boxed region is shown in the right panel. Scale bars, 10 μm (left panel) and 3 μm (right panels). (D) Live-cell imaging of COS-7 cells transfected with GFP-COL3A1 (green) and Golgi-BFP (blue). Images were acquired every 15 min by fluorescence microscopy. Time points indicate minutes of incubation with ascorbate. Cis-Golgi is indicated by arrows. Scale bar, 10 μm. (E) Live-cell imaging of COS-7 cells (left panel) and RD cells (right panel) transfected with GFP-COL3A1 after incubation with ascorbate for 10 d (COS-7 cells) or 2 d (RD cells). Arrows indicate GFP-CO3A1 fibrils. Scale bar, 25 μm.

co-localized with mScarlet-RAB1B until they reached the Golgi apparatus (Supplemental Figure S5A and Supplemental Movie 4). Similarly, when ascorbate was added, we detected GFP-COL3A1–containing vesicles merged with the mScarlet-RAB1B signal (Figure 3A and Supplemental Movie 5).

Cargo proteins are often transported in vesicular and tubular carriers (Presley *et al.*, 1997; Watson and Stephens, 2005; Brandizzi and Barlowe, 2013). RAB1 is observed in tubular configurations when associated with the ERGIC/IC (intermediate compartment; Marie *et al.*, 2009; Saraste and Marie, 2018). In RD cells, we frequently detected tubular structures of mScarlet-RAB1B (Figure 3B). GFP-COL3A1 colocalized with the tubular carrier containing mScarlet-RAB1B for transport to the Golgi apparatus (Figure 3B and Supplemental Movie 6). In the same cells, vesicles containing both GFP-COL3A1 and mScarlet-RAB1B were detected. Moreover, vesicles transformed into tubules, and vice versa, indicating that GFP-COL3A1 was transported by both vesicular and tubular carriers containing RAB1B. GFP-α1AT was also carried by tubular structures decorated with mScarlet-RAB1B (Supplemental Figure S5B and Supplemental Movie 10). The proportion of GFP-COL3A1–containing vesicles and tubules colocalized with mScarlet-RAB1B in the presence of ascorbate was comparable to that of GFP-α1AT–containing tubulovesicular structures colocalized with mScarlet-RAB1B (Figure 3C). Together, these results suggest that procollagen III is transported from the ER to the Golgi apparatus by vesicles and tubules accompanied by RAB1, as with conventional cargos.

We next examined the incorporation of ERGIC53 into transport vesicles containing GFP-COL3A1. ERGIC53, a cargo receptor that recognizes specific forms of N-glycan, is widely used as an ERGIC marker (Hauri *et al.*, 2000; Nyfeler *et al.*, 2008). As previously reported, α1AT is recognized by ERGIC53 when exported from the ER (Nyfeler *et al.*, 2008), and as expected, GFP-α1AT–containing vesicles colocalized with mCherry-ERGIC53 (Supplemental Figure S6A and Supplemental Movie 7; Matsui *et al.*, 2020). Similarly, GFP-COL3A1–containing vesicles moved toward the Golgi apparatus and merged with mCherry-ERGIC53 (Figure 4A and Supplemental Movie 8). These results indicate that the GFP-COL3A1–containing cargo includes the ERGIC membrane, reminiscent of conventional ER-to-Golgi transport vesicles. As observed for mScarlet-RAB1B, tubular extensions containing mCherry-ERGIC53 moved toward the Golgi apparatus, and GFP-COL3A1 was transported along with these carriers (Figure 4B and Supplemental Movie 9). GFP-α1AT was also carried by tubular structures containing mCherry-ERGIC53 (Supplemental Figure S6B and Supplemental Movie 11). We carefully quantified the colocalization by manual inspection and found that 86.6% of GFP-α1AT carriers and 63.4% of GFP-COL3A1–containing structures were ERGIC53-mCherry positive (Figure 4C).

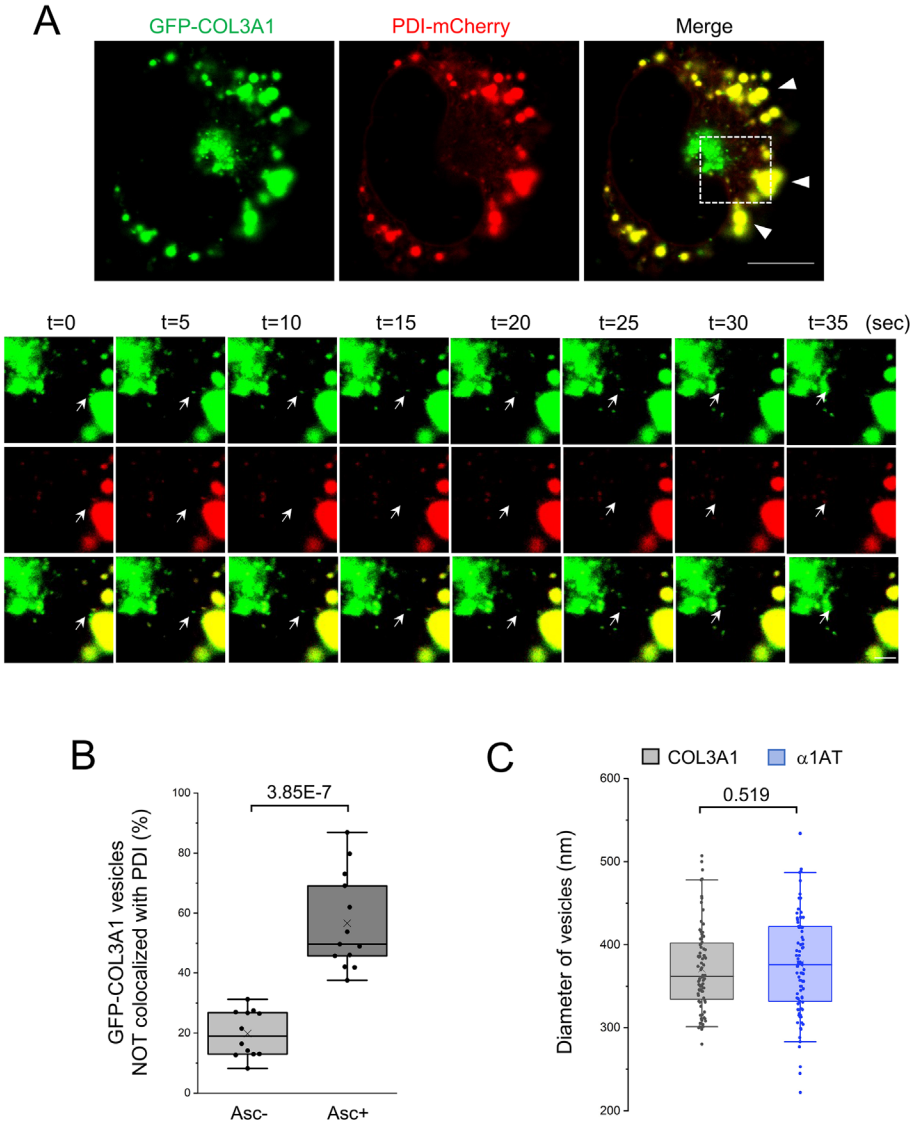

FIGURE 2: Live-cell imaging of ER-to-Golgi trafficking of GFP-COL3A1. (A) Live-cell imaging of RD cells transiently expressing GFP-COL3A1 (green) and PDI-mCherry (red), treated with ascorbate for 1 h. Images were acquired every 5 s by confocal microscopy. Lower panels show higher magnification of the region outlined by the white square (GFP-COL3A1, PDI-mCherry, and the merged images). Arrows indicate vesicles containing GFP-COL3A1 transported toward the Golgi apparatus. Arrowheads denote GFP-COL3A1 accumulated in the ER. Scale bars, 10 μm (upper panels) and 2 μm (lower panels). (B) Quantification of vesicles containing GFP-COL3A1 not colocalized with PDI-mCherry in the absence (Asc-) or presence (Asc+) of ascorbate. Colocalization was analyzed using the ComDet plugin of ImageJ after the Golgi region was excluded from the analysis. Means ± SEM of $n = 12$ and 13 cells in the absence and presence of ascorbate, respectively, from two independent experiments each. The p value is indicated (Mann–Whitney U test). (C) Box plot of diameters of vesicles containing GFP-COL3A1 and GFP-α1AT transported to the Golgi apparatus. Vesicles ($n = 84$ for GFP-COL3A1 and $n = 91$ for GFP-α1AT) in three cells were measured from three independent experiments each. The P value was not statistically significant (two-tailed Student's t test).

Collectively, these observations indicate that GFP-COL3A1 was transported by the vesicular and tubular carriers containing the ER-GIC membrane, as with conventional cargo.

GFP-COL3A1 is cotransported to the Golgi apparatus with α1AT

Because the characteristics of vesicular and tubular carriers of GFP-COL3A1 were reminiscent of those of conventional cargo, we next investigated whether procollagen III was actually transported by conventional transport carriers harboring α1AT. To this end, we cotransfected GFP-COL3A1 and mCherry-α1AT into RD cells. We reasoned that if GFP-COL3A1 and mCherry-α1AT were cotransported in the same vesicle, procollagen III would be likely to use conventional ER-to-Golgi transport carriers. Vesicles containing both GFP-COL3A1 and mCherry-α1AT were transported to the Golgi apparatus (Figure 5 and Supplemental Movie 12). Thus, procollagen III and α1AT were loaded into the same vesicles following fusion with ERGIC shortly after ER exit, or alternatively at the time of budding from the ERES (see the *Discussion*).

Procollagen III undergoes condensation in the endoplasmic reticulum

When ascorbate was added, GFP-COL3A1 expressed in RD cells formed large intracellular puncta (Figures 2A and 6A). The large inclusion emerged ~45 min after the addition of ascorbate (Figure 6A), and most of the GFP signal started to fade ~60 min thereafter. The large GFP-COL3A1 puncta merged with both PDI-mCherry and HSP47-mCherry, indicating that they were highly condensed with the ER folding machinery (Figure 6B). We next investigated whether endogenous procollagen III would form similar structures when ascorbate was added. In the absence of ascorbate, endogenous procollagen III in RD cells was distributed throughout the cytoplasm as small dots colocalized with HSP47 (Figure 6C, Asc-). However, when cells were cultured in the presence of ascorbate, the small scattered structures (Figure 6C, Asc-) appeared to merge, forming large puncta (Figure 6C, Asc+, quantified in Figure 6D). Importantly, ascorbate was present for 48 h before cell staining. A portion of cells cultured in the presence of ascorbate for up to 3 wk contained large droplets (Supplemental Figure S7), indicating that the foci of procollagen III were physiological structures generated during the secretion process.

To determine whether the large foci represented aggregates of terminally misfolded procollagen III or phase-separated intermediates, we performed fluorescence recovery after photobleaching (FRAP) experiments. After a small portion of a large punctum was bleached, the GFP signal recovered rapidly in ~10 s and reached the same fluorescence intensity as before bleaching (Figure 6, E and F, and Supplemental Movie 13). When a half area of a large punctum was bleached, the fluorescence intensity recovered to approximately half of the prebleaching intensity within ~1 min (Supplemental Figure S8A). Fluorescence recovery occurred very slowly when whole puncta were bleached (Supplemental Figure S8B). Together, these results revealed that

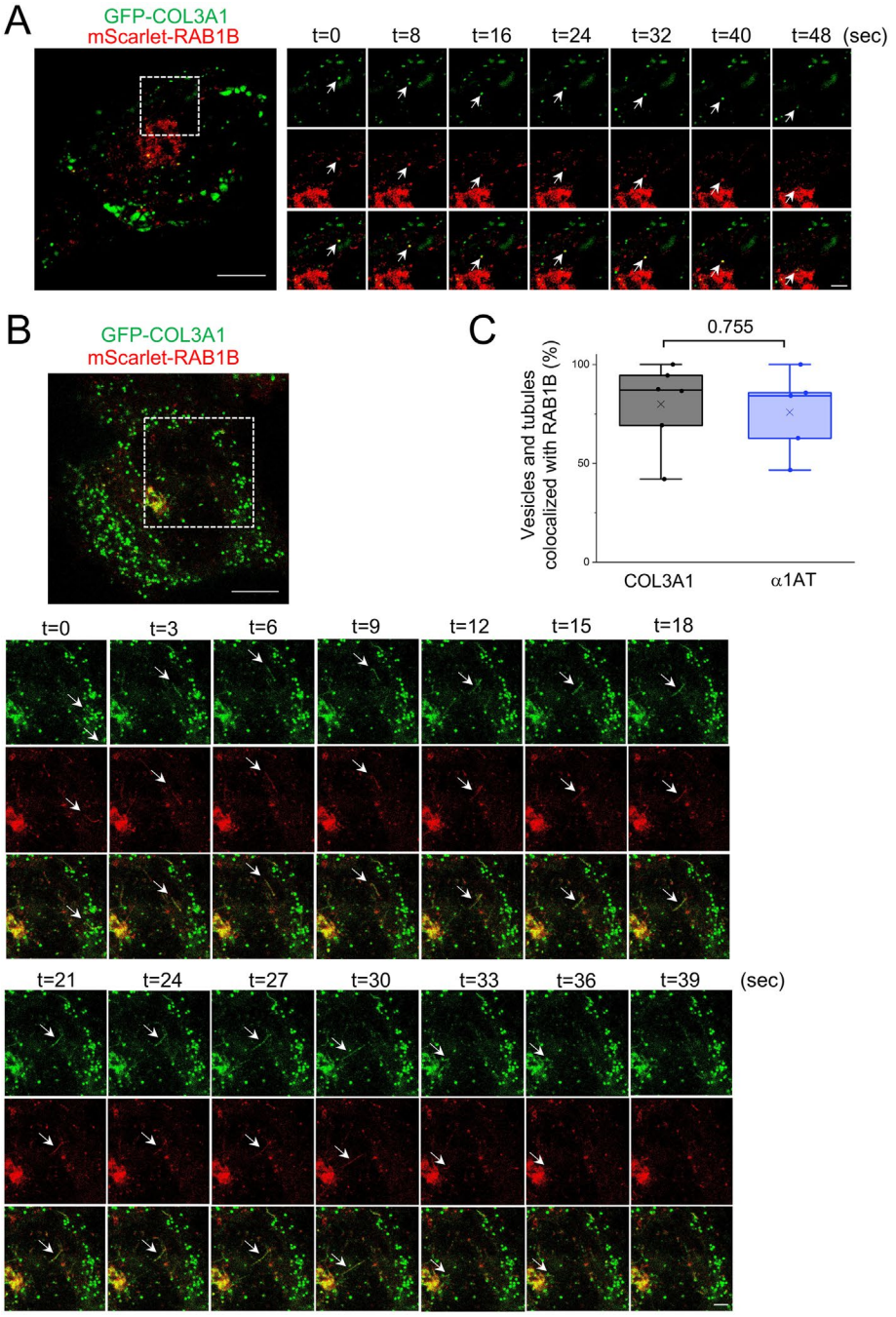

FIGURE 3: GFP-COL3A1 is transported by vesicles and tubules containing mScarlet-RAB1B. (A) Live-cell imaging of RD cells transiently expressing GFP-COL3A1 (green) and mScarlet-RAB1B (red), treated with ascorbate for 1 h. Images were acquired every 4 s by confocal microscopy. Right panels show time-lapse images of the region outlined by the white dotted square (GFP-COL3A1, mScarlet-RAB1B, and the merged images). Arrows indicate GFP-COL3A1 vesicles transported toward the Golgi region. Scale bars, 10 μm (left panel) and 3 μm (right panels). (B) Same as in (A), except for cells containing tubular carriers of GFP-COL3A1 (green) and mScarlet-RAB1B (red). Scale bars, 10 μm (upper panel) and 3 μm (lower panels; GFP-COL3A1, mScarlet-RAB1B, and the merged images). (C) Quantification of vesicles and tubules containing GFP-COL3A1 or GFP-α1AT colocalized with mScarlet-RAB1B. The colocalization was manually inspected on 95 vesicles/tubules in six cells in three independent experiments (GFP-COL3A1) and 128 vesicles/tubules in five cells in four independent experiments (GFP-α1AT), The *p* value was not statistically significant (two-tailed Student's *t* test).

procollagen III molecules in large foci were largely mobile, suggesting that they undergo condensation similar to the liquid–liquid phase separation in the ER together with chaperone proteins.

Live-cell imaging suggested that transport vesicles of GFP-COL3A1 emerged from the large droplets (Figure 2A and Supplemental Movie 2). To further confirm that procollagen III molecules in the large droplets are destined for secretion, we analyzed SEC23, a marker of the ERES. Immunostaining revealed that the droplets were surrounded by SEC23 puncta (Figure 6G), suggesting that the large droplets of GFP-COL3A1 recruited ERES. Consistent with the FRAP result, these observations also suggested that the large droplets of GFP-COL3A1, as well as those of endogenous procollagen III, are not terminally misfolded aggregates but instead represent a fraction of molecules that properly maturate to exit from the ER.

We next investigated whether the observed phase separation–like condensation is unique to type III procollagen or occurs only in RD and COS-7 cells. To this end, we expressed GFP collagens in HT-1080 and HeLa cells, which produce endogenous procollagen IV but not procollagen III. Upon addition of ascorbate, similar large droplets of GFP-COL3A1 were formed in both cell lines, whereas GFP-tagged COL4A1 (Matsui *et al.*, 2020) was expressed in a fine reticular network (Supplemental Figure S8C), suggesting that the drastic condensation by a phase separation–like process is inherent in procollagen III and occurs in other cell lines.

Accumulated GFP-COL3A1 is exported from the endoplasmic reticulum exit site surrounding procollagen III droplets

Previous studies have reported that procollagen I exits from the ERES or in close proximity to that site (Stephens and Pepperkok, 2002; Mironov *et al.*, 2003). TANGO1 forms rings at the ERES for export of collagen VII in human cells (Raote *et al.*, 2017) and collagen IV in *Drosophila* (Liu *et al.*, 2017). Hence, we investigated whether GFP-COL3A1 is exported from the ERES surrounding the droplets. After incubation with ascorbate for 30 min, the cells were cultured at 15°C for 3 h to arrest intracellular transport. By returning the cells to 37°C, ER-to-Golgi transport was reinitiated synchronously. Cells were fixed and immunostained with anti-SEC23 antibody after incubation at 15°C for 3 h (Figure 7A) or 30 min after the temperature shift to 37°C (Figure 7B). When ER-to-Golgi transport was inhibited at 15°C, SEC23 was detected around the large droplets of GFP-COL3A1, adjacent to their margins (Figure 7A, arrowheads). Thirty minutes after the restart of ER-to-Golgi transport, some of the SEC23 signals merged with those of GFP-COL3A1 in the puncta (Figure 7, B–D). Although the number of

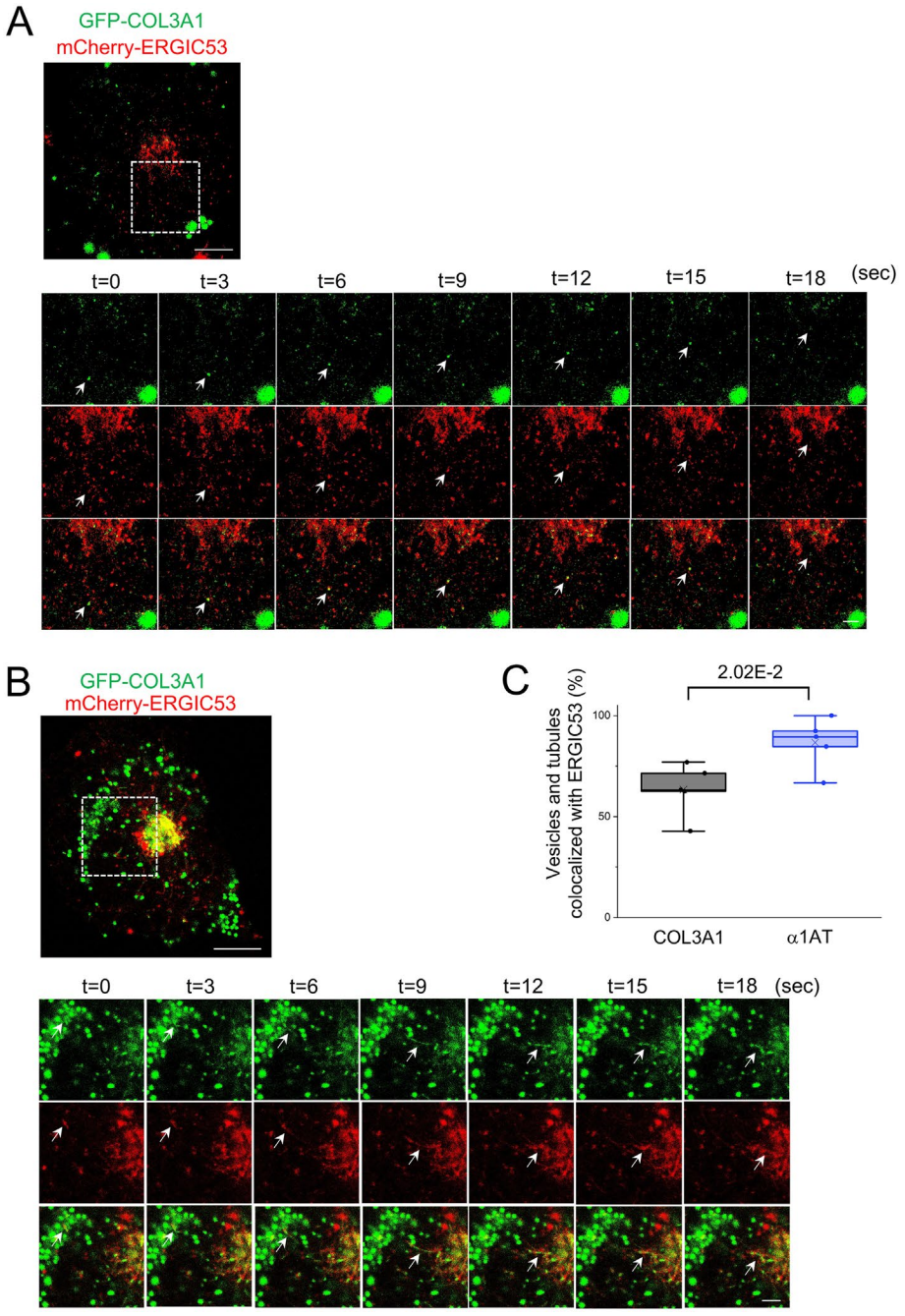

FIGURE 4: GFP-COL3A1 is transported by tubulovesicular carriers containing mCherry-ERGIC53. (A) Same as in Figure 3A, except for cells transiently expressing GFP-COL3A1 (green) and mCherry-ERGIC53 (red) treated with ascorbate for 1 h. Images were acquired every 3 s by confocal microscopy. Right panels show higher magnification of the region outlined by the white dotted square (GFP-COL3A1, mCherry-ERGIC53, and the merged images). Arrows indicate GFP-COL3A1 vesicles transported toward the Golgi region. Scale bars, 10 μm (left panel) and 3 μm (right panels). (B) Same as in Figure 3B, except for cells transiently expressing GFP-COL3A1 (green) and mCherry-ERGIC53 (red). Scale bars, 10 μm (upper panel) and 3 μm (lower panels). (C) Same as in Figure 3C, except for vesicles and tubules co-localized with mCherry-ERGIC53. The colocalization was manually analyzed on 100 vesicles/tubules in five cells in four independent experiments (GFP-COL3A1) and 65 vesicles and tubules in five cells in four independent experiments (GFP-α1AT). The *p* value is indicated (two-tailed Student's *t* test).

puncta that merged with SEC23 was small, there was a difference between the percentage at 0 h and that at 30 min–1 h after the temperature shift to 37°C; it was 1.17% at 0 h (1802 puncta in 19 cells in three independent experiments) and 4.91% at 30 min–1 h after the temperature shift (1772 puncta in 14 cells in three independent experiments). These results suggest that COPII components were clustered in the ER region surrounding the GFP-COL3A1 droplets.

Sar1, TANGO1, and CUL3 are required for the export of procollagen III from the endoplasmic reticulum

Sar1 is a small GTPase that regulates the budding of COPII vesicles from the ERES (Sato and Nakano, 2007; Miller and Barlowe, 2010). To determine whether Sar1 was required for the export of procollagen III from the ER, we transfected the Sar1[H79G] dominant-negative mutant to RD cells. Sar1[H79G] decreased the endogenous procollagen III secreted into the medium and reciprocally increased procollagen III retained in the cells (Figure 8, A–C). TANGO1, a cargo receptor for collagens that is required for the export of other bulky cargos, localizes at the ERES (reviewed in Raote and Malhotra, 2021). However, the requirement of TANGO1 for the export of collagens from the ER depends on collagen type. To analyze the effect of TANGO1 on the secretion of procollagen III, we knocked down TANGO1 using siRNA in RD cells. In cells treated with siTANGO1, the level of procollagen III secreted into the medium was reduced, and the protein was instead retained in the cell lysate (Figure 8, D–F). TANGO1 expression was suppressed to 5–15% of that in control cells (Figure 8D). These results suggest that procollagen III is transported from the ERES and requires TANGO1 for export.

Several other factors are also involved in procollagen transport from the ER. The ubiquitin–ligase complex CUL3-KLHL12 is necessary for procollagen I export from the ER; specifically, the complex enlarges the COPII vesicles to accommodate the rigid procollagen I molecules (Jin *et al.*, 2012). SLY1/SCFD1, which regulates the membrane fusion, and an ER t-SNARE, STX18, are required for the secretion of procollagen VII and II, but not for the export of procollagen I (Nogueira *et al.*, 2014; Hou *et al.*, 2017). TFG organizes the budding of COPII vesicles at the ERES for the transport of procollagen I (McCaughey *et al.*, 2016), and the NRZ complex, which contains ZW10, tethers ERGIC to the ERES for the secretion of procollagen VII (Raote *et al.*, 2018). Sedlin, a component of the TRAPPII complex, regulates the GTP–GDP cycle of SAR1 and RAB1 and is required for the transport of procollagen I and II (Venditti *et al.*, 2012). We analyzed procollagen III secretion in RD cells treated with siRNA targeting

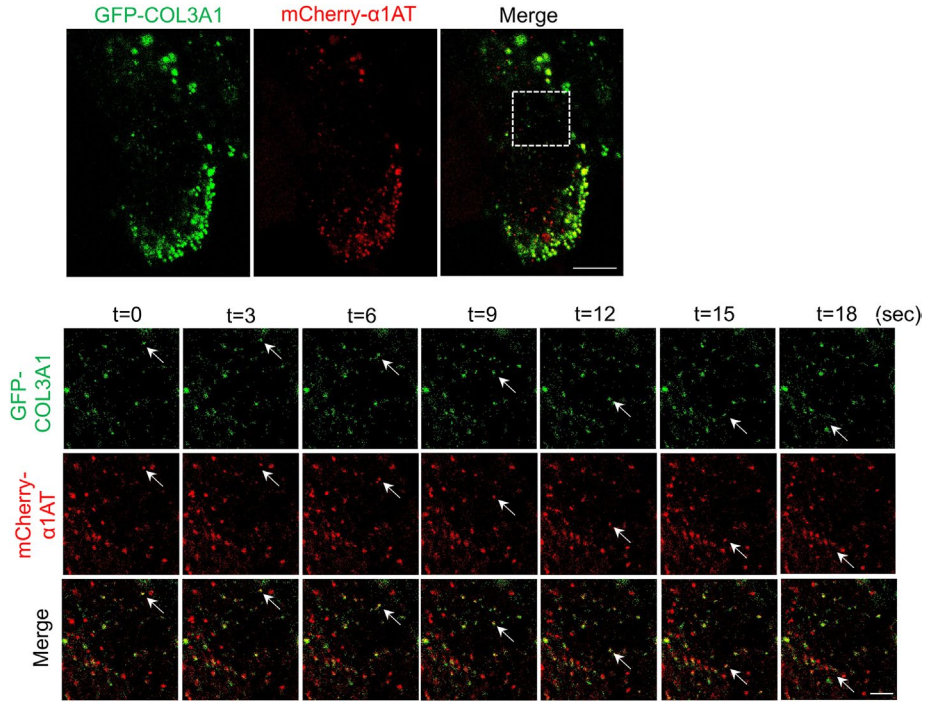

FIGURE 5: GFP-COL3A1 is cotransported from the ER to the Golgi apparatus with mCherry-α1AT. Live-cell imaging of RD cells transiently expressing GFP-COL3A1 (green) and mCherry-α1AT (red) treated with ascorbate for 1 h. Time-lapse images were obtained every 3 s by confocal microscopy. Lower panels show higher magnification of the region outlined by the white dotted square (GFP-COL3A1, mCherry-α1AT, and the merged images). Arrows indicate vesicles containing both GFP-COL3A1 and mCherry-α1AT transported toward the Golgi apparatus. Scale bars, 10 μm (upper panel) and 3 μm (lower panels).

these factors. Because the knockdown efficiency of siSedlin was insufficient, we used siRNA-targeted BET3, another component of the TRAPP complex (Yu *et al.*, 2006). Knockdown of CUL3 significantly inhibited the secretion of procollagen III (Figure 9, A, B, and D). However, other factors, including KLHL12, were not required under our experimental conditions (Supplemental Figure S9, A–D; see *Discussion*). Cells treated with siZW10 secreted higher levels of procollagen III. Knockdown efficiency was ~95% for CUL3 and TFG, ~75% for STX18, ~70% for KLHL12, ~65% for SLY1, ~60% for BET3, and ~50% for ZW10 (Figure 9C and Supplemental Figure S9E). Taking all these together, our analysis suggested that export of procollagen III from the ER requires enlarged COPII vesicles.

DISCUSSION

By constructing a GFP-tagged pro-α1(III) chain that can form extracellular fibrils, we analyzed the ER-to-Golgi transport of procollagen III by live-cell imaging in RD cells, which endogenously synthesize procollagen III. We found that GFP-COL3A1 was transported in vesicular and tubular carriers containing the ERGIC membrane that cotransported GFP-α1AT, a conventional cargo. The diameter of the transport vesicles was 350–400 nm (Figure 2C). Generally, conventional cargos exit the ER in COPII vesicles 60–80 nm in diameter and fuse to the ERGIC compartment shortly after ER exit (Figure 9E, i). Therefore, we propose that the diameter of COPII vesicles in those cells increases in size to >350 nm in order to accommodate procollagen III (Figure 9D, ii), based on the recent studies of collagen secretion (Jin *et al.*, 2012; Malhotra and Erlmann, 2015). Our identification of CUL3 as a factor required for secretion (Figure 9D) supports this model, as CUL3 monoubiquitinates Sec31 in complex with KLHL12 to enlarge COPII vesicles (Jin *et al.*, 2012). However, KLHL12 was not required in our current assay (Figure 9D). Considering the ~70% knockdown efficiency of KLHL12, the residual amount of protein would be sufficient for it to perform its cellular function. Alternatively, it is possible that the CUL3 complex containing a molecule other than KLHL12 is responsible for the generation of enlarged COPII vesicles carrying procollagen III. Conventional cargo such as GFP-α1AT is likely included in those vesicles by default.

Recently, a mechanism was proposed for procollagen I transport: a model of a short loop from the ER to Golgi in which direct tunnel-like structures that can accommodate procollagen I are formed between the ER and Golgi (Figure 9E, iii; McCaughey *et al.*, 2018). However, in cells such as RD cells that produce a large number of collagens, procollagens are synthesized throughout the ER, including the periphery. The ERES mostly surrounded large droplets containing procollagen III (Figure 7), and the majority of ERGIC was located near the perinuclear Golgi-like region (e.g., Figure 4). In this spatial configuration, it seems unlikely that a long direct tunnel from the ERES to ERGIC/Golgi apparatus is the major pathway for procollagen III. We do not exclude the possibility that a direct tunnel is formed between the ER and peripheral ERGIC, procollagen III is still transported by vesicular carriers. Our analyses revealed that large transport carriers also formed from the ERGIC, and that procollagen III was further sorted to the Golgi apparatus in vesicles of 350–400 nm in diameter, which also contained conventional cargos (Figure 9E, v). The colocalization of ERGIC53 and RAB1B on the transport vesicles of procollagen III (Figure 3 and 4) is also consistent with this possibility. We did not detect colocalization of GFP-COL3A1 puncta with LC3-mCherry or LAMP1-mCherry (unpublished data), which represents vesicles destined for degradation via microautophagy (Omari *et al.*, 2018). Sec23-mCherry signals were frequently found at the edge of the GFP-COL3A1 droplets (data not shown).

The pre-Golgi maturation mechanisms of procollagen III (this study) and IV (Matsui *et al.*, 2020), the latter of which involves ER-to-Golgi transport vesicles, were surprisingly different, although both transport carriers had a diameter of ~400 nm. The most striking feature of procollagen III after addition of ascorbate was the induction of condensation, similar to the liquid–liquid phase separation in the ER (Figure 6). Phase separation is an emerging concept in dynamic cellular structures and a major principle underlying the formation of various membraneless organelles (Uversky, 2017; Zhao and Zhang, 2020); in addition, it has been implicated in the pathogenesis of neurodegenerative diseases (Zbinden *et al.*, 2020). In the secretory pathway, immunoglobulin-secreting cells contain large inclusions called Russel bodies (Kopito and Sitia, 2000). Formation of the inclusion is largely dependent on the aggregation properties of misfolded IgG (Valetti *et al.*, 1991), and similar inclusions in the ER are considered to represent liquid–liquid phase separation of highly condensed proteins (Hasegawa *et al.*, 2015). In this study, we found

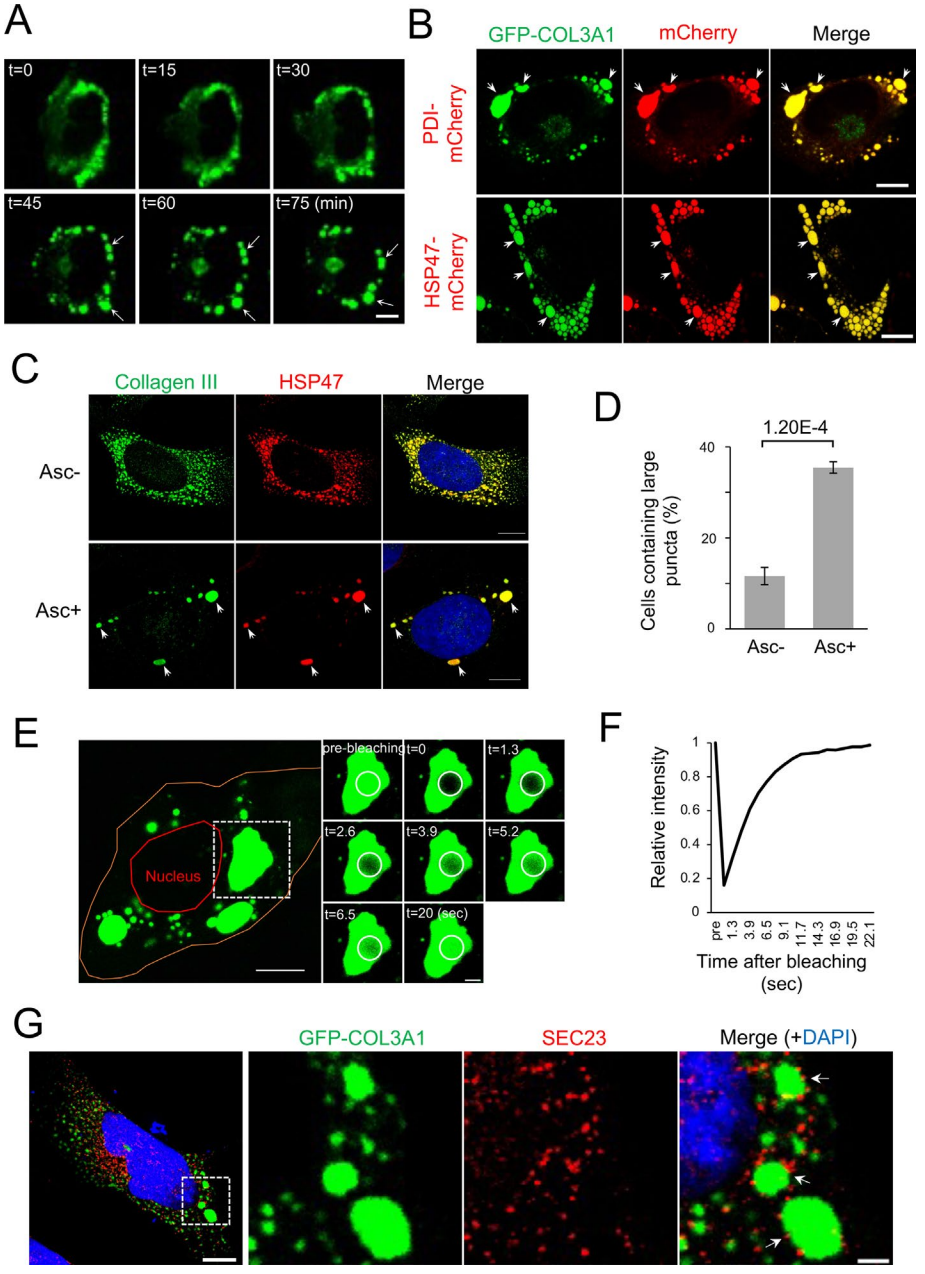

FIGURE 6: Procollagen III undergoes liquid–liquid phase separation–like events in the ER upon ascorbate addition. (A) Live-cell imaging of RD cells transfected with GFP-COL3A1 (green). Time-lapse images were acquired by fluorescence microscopy every 15 min after the addition of ascorbate. Large puncta containing GFP-COL3A1 are indicated by arrows. Scale bar, 10 μm. (B) Live-cell imaging of RD cells transiently expressing GFP-COL3A1 (green) and PDI-or HSP47-mCherry (red) treated with ascorbate for 1 h. Arrows are the same as in A. Scale bar, 10 μm. (C) Immunostaining of RD cells. After incubation with ascorbate for 2 d, cells were fixed and stained with anti-pN(III) (green) and anti-HSP47 (red) antibodies. Arrows indicate large puncta containing procollagen III. Scale bar, 10 μm. (D) Quantification of cells containing at least one large punctum of procollagen III (>1 μm in diameter) in (C). Mean ± SEM of 34 (Asc-) and 38 fields (Asc+) containing 5–35 cells from three independent experiments. The *P* value is indicated (two-tailed Student's *t* test). (E) FRAP experiment of RD cells transiently expressing GFP-COL3A1. Right panels show the higher magnification of the region outlined by the white dotted box. Images were acquired every 1.3 s after photobleaching. Relative fluorescence intensity is shown in the graph. Orange and red lines indicate the outlines of the cell and nucleus, respectively. White circles show the bleached area. Scale bars, 10 μm (left panel) and 3 μm (right panels). (F) Quantification of the fluorescence intensity in the white circle shown in (E). (G) Immunostaining of RD cells transiently expressing GFP-COL3A1. After incubation with ascorbate for 2 d, cells were fixed and stained with anti-GFP (green) and anti-SEC23 (red) antibodies. Right panels show higher magnification of the region outlined by the white dotted square. Arrows indicate SEC23 located adjacent to the large GFP-COL3A1 puncta. Scale bars, 10 μm (whole cell) and 3 μm (enlarged, right panels).

that 4-hydroxylation of proline residues remodeled the scattered distribution of GFP-COL3A1, as well as native procollagen III, into mobile droplets. Interestingly, the intracellular accumulation of procollagen II, similar to that of procollagen III droplets, has been reported as "rough ER (RER) sacs" that are generated in chondrocytes after the addition of ascorbate (Pacifici and Iozzo, 1988). Because the RER sacs were also detected in the absence of ascorbic acid by lowering the temperature to 23°C, the authors speculate that procollagen hydroxylation and helix formation precede RER remodeling. In general, 4-hydroxyproline in mature collagen molecules confers additional thermal stability on the triple helix, probably by introducing additional hydrogen bonds and rearranging the surrounding water network (Bella, 2016). The modification of procollagen III molecules may also increase the chance of intermolecular hydrogen bond formation and decrease hydration, leading to phase separation–like events. At a minimum, because (i) PDI and HSP47 were co-condensed and (ii) the ERES was found in close proximity to the droplets, the separation likely generates environments favorable for efficient structural rearrangement, which is required for the packaging of procollagen III in COPII vesicles. In procollagen IV, we observed no obvious phase separation. This may be related to the differential requirements of transport factors as described. For example, TANGO1 and CUL3 were necessary for procollagen III but not IV (Matsui *et al.*, 2020). Further analysis is required to determine whether collagens other than procollagen II and III form such structures, and whether it depends on the level of condensation and rate of synthesis in the ER. Furthermore, it is worth analyzing whether such phase separation–like events are required for the quality control of newly synthesized procollagens.

MATERIALS AND METHODS

Request a protocol through *Bio-protocol*.

Plasmid construction

The human *COL3A1* gene was kindly provided by T. Sasaki (Oita University, Japan). To construct GFP-COL3A1, an 861 bp *Bam*HI fragment of the human *COL3A1* gene containing the N-telopeptide region was first subcloned into pBlueScript, and

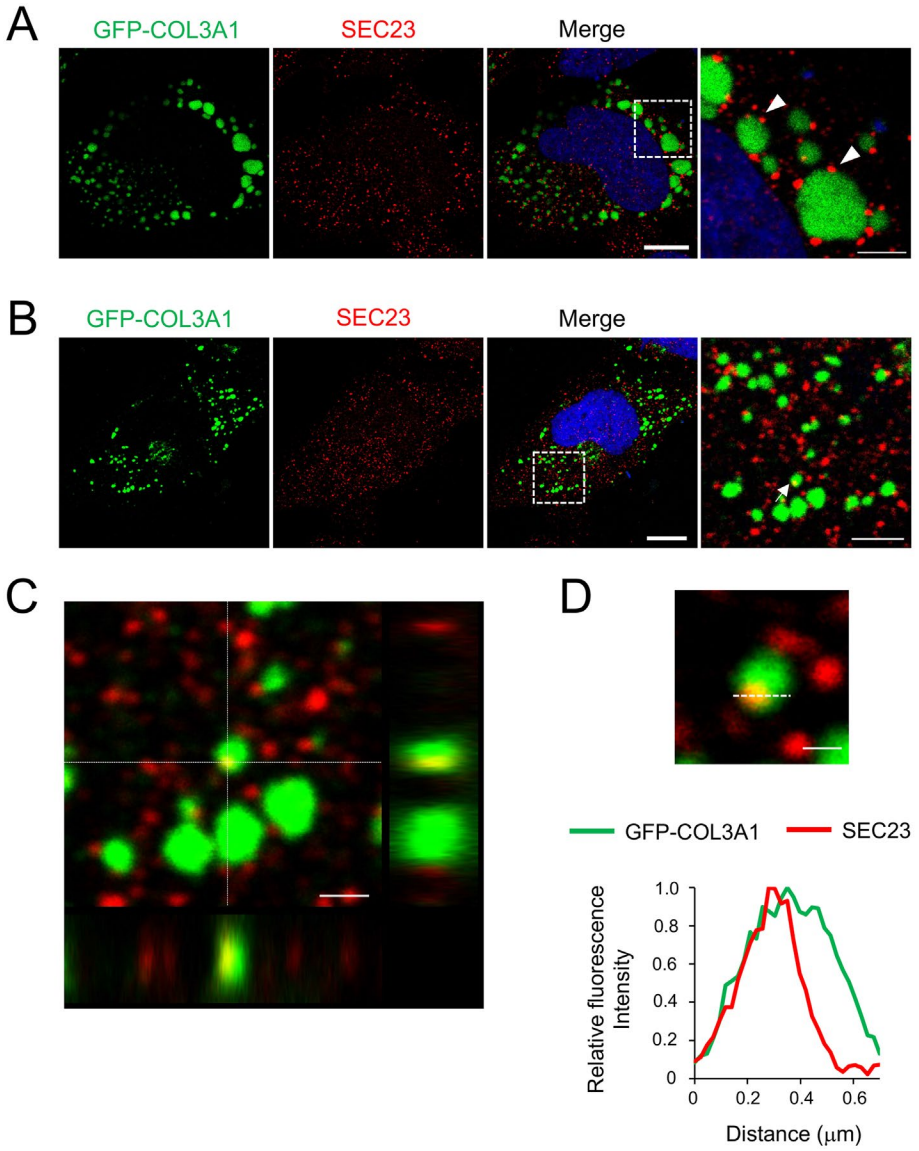

FIGURE 7: Procollagen III is exported from the ER exit sites. (A) Immunostaining of RD cells transiently expressing GFP-COL3A1. After incubation with ascorbate for 30 min, cells were cultured at 15°C for 3 h and stained with anti-GFP (green) and anti-SEC23 (red) antibodies. Higher magnification of the region outlined by the white dotted square is shown in the right panel. Arrowheads indicate SEC23 signals detected adjacent to large puncta containing GFP-COL3A1. Scale bars, 10 μm (left panels) and 3 μm (magnified, rightmost panel). (B) Same as in A, except that after incubation at 15°C for 3 h, cells were returned to 37°C and cultured for 30 min. (C) Colocalization of GFP-COL3A1 and SEC23. A punctum indicated by an arrow in B was magnified, and images of the *X–Z* and *Y–Z* axes are shown. Scale bar, 1 μm. (D) Line-scan analysis of the fluorescence intensities of GFP-COL3A1 (green) and SEC23 (red). Scale bar, 0.5 μm.

cfSGFP2 lacking Met was PCR-amplified and inserted into the *Nde*I site within the N-telopeptide region using InFusion (Clontech/Takara Bio USA, Mountain View, CA, USA). The 3′ and 5′ flanking sequences were sequentially subcloned into pcDNA3.1, and the *Bam*HI fragment containing cfSGFP2 was inserted. To generate HSP47-mCherry, the KDEL ER retrieval sequence was first introduced to the C-terminus of mCherry-N1 (Clontech), and then mouse HSP47 lacking the RDEL ER retrieval signal was inserted into the N-terminus of mCherry. To construct mScarlet-RAB1B, cDNA encoding RAB1B was first subcloned into the *Eco*RI–*Bam*HI site of cfSBFP2, which contains a flexible linker sequence encoding SGSTGSTGSTG between the *Bsp*EI and *Xho*I sites, and then the *Age*I–*Bsr*GI fragment of cfSBFP2 was replaced with the *Age*I–*Bsr*GI fragment of mScarlet. To generate mCherry-α1AT, mCherry lacking the stop codon was inserted into the pCMV-Tag4 vector containing the signal sequence of α1AT, and then α1AT lacking the signal sequence was inserted at the C-terminus of mCherry. PDI-mCherry, Golgi-BFP, mCherry-ERGIC53, and GFP-α1AT were constructed as described previously (Matsui *et al.*, 2020).

The Sar1[H79G] mutant containing EYFP at the N-terminus was constructed from the SAR1 expression vector (Kamada *et al.*, 2004). Briefly, the human SAR1 cDNA was recloned into the *Xho*I–*Eco*RI sites of EYFP-C1, and a point mutation was created by overlapping PCR to convert His79 to Gly.

siRNA oligos

The siRNA oligo sequences used were as follows: TANGO1, 5′-GAUAAGGUCUUCCGUGCUUTT-3′ (Santos *et al.*, 2015); BET3, 5′-UCACUCCAAGCAUUACUAAUUTT-3′ (Yu *et al.*, 2006); SLY1/SCFD1, 5′-AGACUUAUUGAUCUCCAUATT-3′ (Nogueira *et al.*, 2014); STX18, 5′-CAGGACCGCUGUUUUGGAUUUTT-3′ (Nogueira *et al.*, 2014); ZW10, 5′-UGGACGAUGAAGAGAAUUATT-3′ (Raote *et al.*, 2018); and TFG, 5′-ACUUCUGAGUAAUGAUGAATT-3′ (McCaughey *et al.*, 2016). The sequences used for CUL3 and KLHL12 are described elsewhere (Matsui *et al.*, 2020). Medium GC negative-control siRNA (Invitrogen, Waltham, MA, USA) was used as a control siRNA.

Antibodies

A rabbit polyclonal antibody against the N-propeptide of human procollagen III [pN(III)] was provided by T. Sasaki (Nowack *et al.*, 1976). Rabbit anti-GFP antibody was generated as described previously (Sakurai *et al.*, 2018). Other validated antibodies used were rabbit anti-collagen type III (N-terminal; 22734-1-AP, Proteintech, Rosemont, IL, USA), mouse anti-GFP (11814460001, Roche Applied Science, Mannheim, Germany), mouse anti-MIA3/TANGO1 (sc-393916, Santa Cruz Biotechnology, Dallas, TX, USA), mouse anti-CUL3 (sc-166110, Santa Cruz Biotechnology), mouse anti-KLHL12 (sc-514874, Santa Cruz Biotechnology), rabbit anti-SLY1/SCFD1 (CSB-PA840987ESR2HU, CUSABIO Technology, Wuhan, China), mouse anti-STX18 (sc-293067, Santa Cruz Biotechnology), mouse anti-TFG (66919-1-Ig, Proteintech), mouse anti-ZW10 (sc-81430, Santa Cruz Biotechnology), rabbit anti-TRAPPC3/BET3 (CSB-PA000993, CUSABIO Technology), mouse anti-actin (MAB1501, Millipore, Billerica, MA, USA), rabbit anti-calnexin (SPA-860, Enzo Life Sciences, Farmingdale, NY, USA), mouse anti-HSP47 (SPA-470, Enzo Life Sciences), rabbit anti-SEC23 (PA1-069, Affinity BioReagents, Golden, CO, USA), mouse

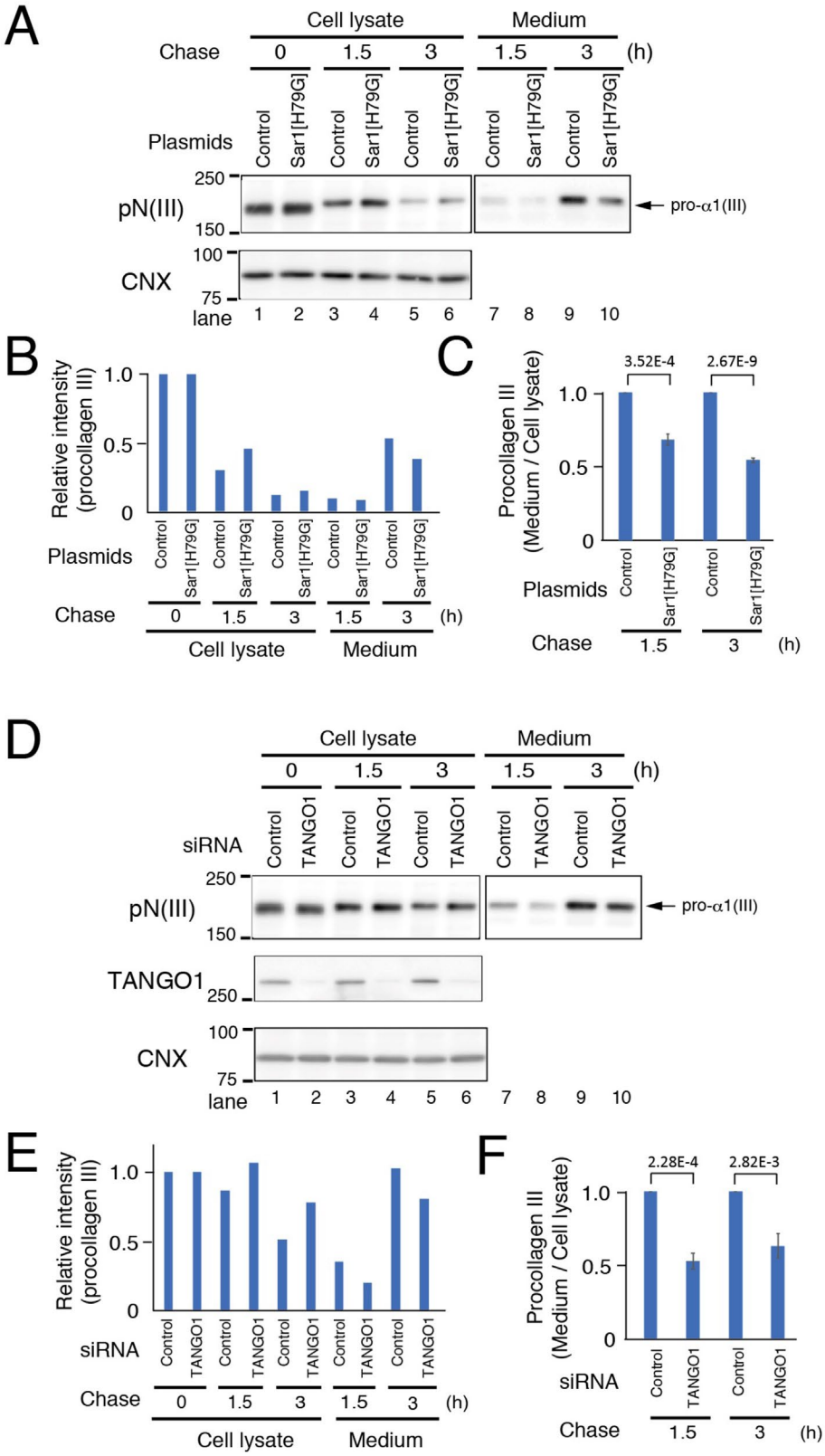

FIGURE 8: Sar1 and TANGO1 are required for GFP-COL3A1 export from the ER. (A) Twenty-four hours after the transfection of the Sar1[H79G] mutant, RD cells were cultured in SFM containing CHX and ascorbate and were chased for the indicated periods. The arrow indicates pro-α1(III) in the cell lysate and culture medium analyzed by Western blotting. Calnexin (CNX) was used as a loading control. Representative blots from three independent experiments are shown. (B) Quantification of relative intensity of pro-α1(III) in A. (C) Medium/cell lysate ratio of pro-α1(III) in A was normalized to that of mock-transfected cells (Control). Mean ± SD of three independent experiments. *p* values (two-tailed Student's *t* test) are indicated. (D) Same as in A, except for cells treated with siRNA for 48 h. Representative blots from three independent experiments are shown. (E) Quantification of relative intensity of pro-α1(III) in D. (F) Medium/lysate ratio of pro-α1(III) in D was normalized to that of negative-control siRNA-transfected cells (Control). Mean ± SD of three independent experiments. *P* values (two-tailed Student's *t* test) are indicated.

anti-GM-130 (610823, BD Biosciences, Franklin Lakes, NJ, USA), horseradish peroxidase-conjugated anti-rabbit IgG (BTI-572, BTI; Thermo Fisher Scientific, Rockford, IL, USA), horseradish peroxidase-conjugated anti-mouse IgG (61-6520, Zymed Laboratories/Thermo Fisher Scientific), Alexa Fluor 594-conjugated goat anti-rabbit IgG (ab150084, Abcam, Cambridge, UK), and Alexa Fluor 488-conjugated goat anti-mouse IgG (ab150117, Abcam).

Cell culture, transfection, and drug treatment

Cells were grown in DMEM supplemented with 10% fetal bovine serum. RD human rhabdomyosarcoma cell line (ATCC; CCL-136) and the HT-1080 human osteosarcoma cell line (ATCC; CCL-121) were provided by Klaus Kuhn (Max Planck Institute, Germany). COS-7 and HeLa cells were purchased from JCRB (Osaka, Japan; JCRB9127 COS-7) and ATCC (CRM-CCL-2), respectively. All cells were confirmed free from mycoplasma infection. TransIT LT1 (Takara, Otsu, Japan) and RNAi-MAX (Invitrogen) were used for the transfection of plasmids and siRNA, respectively. To induce ER-to-Golgi transport of procollagen III and GFP-COL3A1, ascorbic acid phosphate (Wako, Osaka, Japan) was added to the medium at a final concentration of 136 μg/ml. Cycloheximide (Nacalai Tesque, Kyoto, Japan) was dissolved in phosphate-buffered saline and added to the medium at a final concentration of 100 μM. To inhibit the ER-to-Golgi transport by temperature shift, culture medium was replaced with MEM with Hanks's balanced salt solution (Thermo Fisher Scientific) precooled at 15°C, and the cells were incubated in a normal incubator without CO_2 supply. To restart ER-to-Golgi traffic, the medium was replaced with DMEM prewarmed at 37°C and returned to a CO_2 incubator set at 37°C.

Live-cell imaging

Live-cell imaging was performed as described previously (Matsui *et al.*, 2020). Briefly, cells were grown on 35-mm

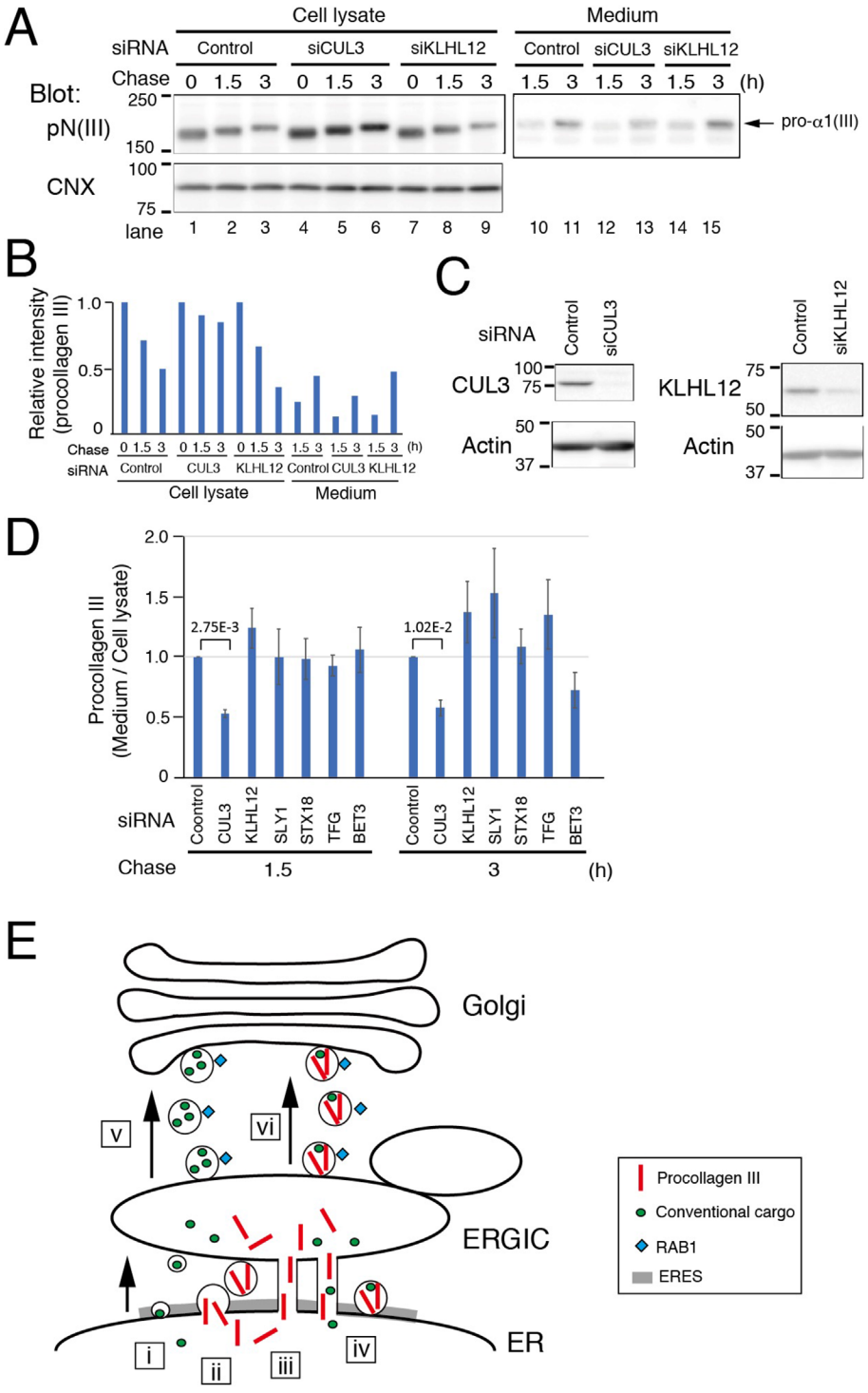

FIGURE 9: CUL3 is required for the GFP-COL3A1 transport from the ER. (A) Forty-eight hours after siRNA treatment, RD cells were cultured in SFM containing CHX and ascorbate, and were chased for the indicated periods. The arrow indicates pro-α1(III) in the cell lysate and culture medium analyzed by Western blotting. Representative blots from three independent experiments are shown. (B) Quantification of the relative intensity of pro-α1(III) in A. (C) Western blot analysis of RD cells treated with siRNA targeting CUL3 and KLHL12 for 48 h. Actin was used as a loading control. Representative blots from three independent experiments are shown. (D) The medium/cell lysate ratio of pro-α1(III) in A and Supplemental Figure S8 was normalized to that of negative-control siRNA-treated cells (Control). Means ± SD of three independent experiments. *P* values (two-tailed Student's *t* test) are indicated. (E) Scheme of procollagen III secretion. Conventional cargos such as α1-AT are transported from the ER exit site (ERES) via COPII vesicles with a diameter of 60–80 nm (i). Transport vesicles of larger size emerge from the ERGIC to transport the cargo to the Golgi apparatus (v). Procollagen III is exported from the ERES to the ERGIC by an enlarged COPII vesicle (ii) or a tunnel-like structure (iii). Transport vesicles containing both procollagen III and α1-AT emerge from ERGIC (vi). It remains unclear whether α1-AT and procollagen III exit the ER separately or use the same vesicle or transport tunnel (iv).

glass-bottomed dishes and transfected with the indicated plasmids. Images were acquired using a Leica TCS SP8 confocal microscope (Leica Microsystems, Wetzler, Germany) equipped with a 63 × /1.4 N.A. oil immersion objective or with a DMI6000B fluorescence microscope (Leica) equipped with a 40 × /0.75 N.A. objective and were analyzed with LAS AF (Leica). Images obtained from a single confocal plane are shown. The temperature was set to 37°C with 5% CO_2 using a microscope incubator (Tokai Hit, Shizuoka, Japan). To measure vesicle sizes, images (1024 × 1024 pixels) were acquired using a Leica TCS SP8 microscope including the LIGHTNING package, which enables 140-nm resolution by setting the pinhole at 0.5 Airy units and processing the images by deconvolution. The diameters were measured manually. For photobleaching and FRAP experiments, a 100% laser beam was focused on the intended area. Line graph software in LAS AF (Leica) was used to identify vesicles containing two different fluorescent proteins. The ComDet plugin of ImageJ was used to quantify the colocalization of GFP-COL3A1 and PDI-mCherry. Particle size was set between 3 and 10 pixels, so that particles larger than ~200 nm in diameter could be counted. The Golgi region was manually defined to exclude it from the analysis. Colocalization of GFP-COL3A1 and GFP-α1AT with mScarlet-RAB1B or mCherry-ERGIC53 was identified manually so that only the carriers moving to the Golgi region were counted.

Immunocytochemistry

Cells plated on a coverslip were fixed for 15 min with 4% paraformaldehyde at room temperature. After permeabilization for 4 min with 0.2% Triton X-100 on ice, cells were stained with the indicated antibodies. Nuclei were counterstained with DAPI. Fluorescence images were captured through a HC PL APO 63 × (NA 1.4) objective lens at 1024 × 1024 dpi on a TCS SP8 microscope (Leica). Images obtained from a single confocal plane are shown. Colocalization of SEC23 positive structures with the endogenous procollagen III puncta was manually assigned by inspecting all the Z-stack images of each structure.

The number of procollagen III puncta was counted using the Analyze Particles function of ImageJ.

Western blotting

Western blot analysis was performed as described previously (Matsui *et al.*, 2020). Briefly, cells were lysed in a buffer containing 1% NP-40 and protease inhibitors. Cell extracts and culture medium (SFM) dissolved in 1 × Laemmli's buffer containing 0.1 M DTT were separated by SDS–PAGE and blotted onto PVDF membranes (Millipore). After blocking with Blocking-One solution (Nacalai Tesque), the membranes were incubated with antibodies diluted in PBS containing 0.1% Tween-20 and 5% Blocking-One solution. Specific signals were detected using Pierce Western Blotting Substrate (Thermo Fisher Scientific) and visualized on a LAS-4000 (GE Healthcare Bio-Sciences). Signal intensity was quantified using the ImageQuant software.

Metabolic labeling and immunoprecipitation

RD cells transfected with GFP-COL3A1 were metabolically labeled with 8.2 MBq/ml [^{35}S] Protein Labeling Mixture (PerkinElmer Life Sciences) for 1 h and chased for the indicated times. Anti-GFP antibody (Roche) was added to cells lysed in a buffer containing 1% NP-40. Immunoprecipitates collected using Protein-G Sepharose were eluted in Laemmli buffer and separated by 5% SDS–PAGE. Gels were dried and exposed to Imaging plates (Fuji Film/GE Healthcare Bio-Sciences). Radioactive incorporation was visualized using an FLA PhosphorImager (GE Healthcare Bio-Sciences), and the signal intensity of each protein was quantified using ImageQuant software (GE Healthcare Bio-Sciences).

Statistical analysis

All results are indicated by means ± SEM or SD. Numbers of replicates are described in the figure legends. Statistical analysis was performed by two-tailed Student's *t* test or by Mann–Whitney *U* test. $P < 0.05$ was considered statistically significant.

The materials reported in this manuscript will be made available on reasonable request.

ACKNOWLEDGMENTS

We thank T. Sasaki (Oita University, Japan) for kindly providing the human procollagen III cDNA and the rabbit polyclonal antibody [pN(III)] and for discussions about the construction of GFP-COL3A1, Klaus Kuhn (Max Planck Institute, Germany) for kindly providing the RD human rhabdomyosarcoma cell line (ATCC; CCL-136) and the HT-1080 human osteosarcoma cell line (ATCC; CCL-121), and K. Takemoto (Kyoto University) for statistical analysis.

REFERENCES

Aridor M (2018). COPII gets in shape: lessons derived from morphological aspects of early secretion. Traffic 19, 823–839.

Bachinger HP, Doege KJ, Petschek JP, Fessler LI, Fessler JH (1982). Structural implications from an electronmicroscopic comparison of procollagen V with procollagen I, pC-collagen I, procollagen IV, and a *Drosophila* procollagen. J Biol Chem 257, 14590–14592.

Barlowe C, Orci L, Yeung T, Hosobuchi M, Hamamoto S, Salama N, Rexach MF, Ravazzola M, Amherdt M, Schekman R (1994). COPII: a membrane coat formed by Sec proteins that drive vesicle budding from the endoplasmic reticulum. Cell 77, 895–907.

Beck K, Boswell BA, Ridgway CC, Bachinger HP (1996). Triple helix formation of procollagen type I can occur at the rough endoplasmic reticulum membrane. J Biol Chem 271, 21566–21573.

Bella J (2016). Collagen structure: new tricks from a very old dog. Biochem J 473, 1001–1025.

Brandizzi F, Barlowe C (2013). Organization of the ER-Golgi interface for membrane traffic control. Nat Rev Mol Cell Biol 14, 382–392.

Canty EG, Kadler KE (2005). Procollagen trafficking, processing and fibrillogenesis. J Cell Sci 118, 1341–1353.

Fromme JC, Schekman R (2005). COPII-coated vesicles: flexible enough for large cargo? Curr Opin Cell Biol 17, 345–352.

Gordon MK, Hahn RA (2010). Collagens. Cell Tissue Res 339, 247–257.

Hasegawa H, Patel N, Lim AC (2015). Overexpression of cryoglobulin-like single-chain antibody induces morular cell phenotype via liquid–liquid phase separation in the secretory pathway organelles. FEBS J 282, 2777–2795.

Hauri HP, Kappeler F, Andersson H, Appenzeller C (2000). ERGIC-53 and traffic in the secretory pathway. J Cell Sci 113, 587–596.

Hou N, Yang Y, Scott IC, Lou X (2017). The Sec domain protein Scfd1 facilitates trafficking of ECM components during chondrogenesis. Dev Biol 421, 8–15.

Hulmes DJ (2002). Building collagen molecules, fibrils, and suprafibrillar structures. J Struct Biol 137, 2–10.

Jin L, Pahuja KB, Wickliffe KE, Gorur A, Baumgartel C, Schekman R, Rape M (2012). Ubiquitin-dependent regulation of COPII coat size and function. Nature 482, 495–500.

Kamada A, Nagaya H, Tamura T, Kinjo M, Jin HY, Yamashita T, Jimbow K, Kanoh H, Wada I (2004). Regulation of immature protein dynamics in the endoplasmic reticulum. J Biol Chem 279, 21533–21542.

Kopito RR, Sitia R (2000). Aggresomes and Russell bodies. Symptoms of cellular indigestion? EMBO Rep 1, 225–231.

Krieg T, Timpl R, Alitalo K, Kurkinen M, Vaheri A (1979). Type III procollagen is the major collageneous component produced by a continuous rhabdomyosarcoma cell line. FEBS Lett 104, 405–409.

Lee MC, Miller EA, Goldberg J, Orci L, Schekman R (2004). Bi-directional protein transport between the ER and Golgi. Annu Rev Cell Dev Biol 20, 87–123.

Liu M, Feng Z, Ke H, Liu Y, Sun T, Dai J, Cui W, Pastor-Pareja JC (2017). Tango1 spatially organizes ER exit sites to control ER export. J Cell Biol 216, 1035–1049.

Ma W, Goldberg J (2016). TANGO1/cTAGE5 receptor as a polyvalent template for assembly of large COPII coats. Proc Natl Acad Sci USA 113, 10061–10066.

Malhotra V, Erlmann P (2015). The pathway of collagen secretion. Annu Rev Cell Dev Biol 31, 109–124.

Marie M, Dale HA, Sannerud R, Saraste J (2009). The function of the intermediate compartment in pre-Golgi trafficking involves its stable connection with the centrosome. Mol Biol Cell 20, 4458–4470.

Matsui Y, Hirata Y, Wada I, Hosokawa N (2020). Visualization of procollagen IV reveals ER-to-Golgi transport by ERGIC-independent carriers. Cell Struct Funct 45, 107–119.

McCaughey J, Miller VJ, Stevenson NL, Brown AK, Budnik A, Heesom KJ, Alibhai D, Stephens DJ (2016). TFG promotes organization of transitional ER and efficient collagen secretion. Cell Rep 15, 1648–1659.

McCaughey J, Stephens DJ (2019). ER-to-Golgi transport: a sizeable problem. Trends Cell Biol 29, 940–953.

McCaughey J, Stevenson NL, Cross S, Stephens DJ (2018). ER-to-Golgi trafficking of procollagen in the absence of large carriers. J Cell Biol.

Miller EA, Barlowe C (2010). Regulation of coat assembly—sorting things out at the ER. Curr Opin Cell Biol 22, 447–453.

Mironov AA, Mironov AA Jr, Beznoussenko GV, Trucco A, Lupetti P, Smith JD, Geerts WJ, Koster AJ, Burger KN, Martone ME, *et al.* (2003). ER-to-Golgi carriers arise through direct en bloc protrusion and multistage maturation of specialized ER exit domains. Dev Cell 5, 583–594.

Mouw JK, Ou G, Weaver VM (2014). Extracellular matrix assembly: a multiscale deconstruction. Nat Rev Mol Cell Biol 15, 771–785.

Myllyharju J, Kivirikko KI (2004). Collagens, modifying enzymes and their mutations in humans, flies and worms. Trends Genet 20, 33–43.

Nogueira C, Erlmann P, Villeneuve J, Santos AJ, Martinez-Alonso E, Martinez-Menarguez JA, Malhotra V (2014). SLY1 and Syntaxin 18 specify a distinct pathway for procollagen VII export from the endoplasmic reticulum. Elife 3, e02784.

Nowack H, Gay S, Wick G, Becker U, Timpl R (1976). Preparation and use in immunohistology of antibodies specific for type I and type III collagen and procollagen. J Immunol Methods 12, 117–124.

Nyfeler B, Reiterer V, Wendeler MW, Stefan E, Zhang B, Michnick SW, Hauri HP (2008). Identification of ERGIC-53 as an intracellular transport receptor of alpha1-antitrypsin. J Cell Biol 180, 705–712.

Omari S, Makareeva E, Roberts-Pilgrim A, Mirigian L, Jarnik M, Ott C, Lippincott-Schwartz J, Leikin S (2018). Noncanonical autophagy at ER

exit sites regulates procollagen turnover. Proc Natl Acad Sci USA 115, E10099–E10108.
Pacifici M, Iozzo RV (1988). Remodeling of the rough endoplasmic reticulum during stimulation of procollagen secretion by ascorbic acid in cultured chondrocytes. A biochemical and morphological study. J Biol Chem 263, 2483–2492.
Plutner H, Cox AD, Pind S, Khosravi-Far R, Bourne JR, Schwaninger R, Der CJ, Balch WE (1991). Rab1b regulates vesicular transport between the endoplasmic reticulum and successive Golgi compartments. J Cell Biol 115, 31–43.
Presley JF, Cole NB, Schroer TA, Hirschberg K, Zaal KJ, Lippincott-Schwartz J (1997). ER-to-Golgi transport visualized in living cells. Nature 389, 81–85.
Raote I, Malhotra V (2019). Protein transport by vesicles and tunnels. J Cell Biol 218, 737–739.
Raote I, Malhotra V (2021). Tunnels for protein export from the endoplasmic reticulum. Annu Rev Biochem 90, 605–630.
Raote I, Ortega Bellido M, Pirozzi M, Zhang C, Melville D, Parashuraman S, Zimmermann T, Malhotra V (2017). TANGO1 assembles into rings around COPII coats at ER exit sites. J Cell Biol 216, 901–909.
Raote I, Ortega-Bellido M, Santos AJ, Foresti O, Zhang C, Garcia-Parajo MF, Campelo F, Malhotra V (2018). TANGO1 builds a machine for collagen export by recruiting and spatially organizing COPII, tethers and membranes. Elife 7, e32723.
Ricard-Blum S (2011). The collagen family. Cold Spring Harb Perspect Biol 3, a004978.
Saito K, Chen M, Bard F, Chen S, Zhou H, Woodley D, Polischuk R, Schekman R, Malhotra V (2009). TANGO1 facilitates cargo loading at endoplasmic reticulum exit sites. Cell 136, 891–902.
Saito K, Yamashiro K, Ichikawa Y, Erlmann P, Kontani K, Malhotra V, Katada T (2011). cTAGE5 mediates collagen secretion through interaction with TANGO1 at endoplasmic reticulum exit sites. Mol Biol Cell 22, 2301–2308.
Sakurai C, Itakura M, Kinoshita D, Arai S, Hashimoto H, Wada I, Hatsuzawa K (2018). Phosphorylation of SNAP-23 at Ser95 causes a structural alteration and negatively regulates Fc receptor-mediated phagosome formation and maturation in macrophages. Mol Biol Cell 29, 1753–1762.
Santos AJ, Raote I, Scarpa M, Brouwers N, Malhotra V (2015). TANGO1 recruits ERGIC membranes to the endoplasmic reticulum for procollagen export. Elife 4, e10982.
Saraste J, Lahtinen U, Goud B (1995). Localization of the small GTP-binding protein rab1p to early compartments of the secretory pathway. J Cell Sci 108(Pt 4), 1541–1552.
Saraste J, Marie M (2018). Intermediate compartment (IC): from pre-Golgi vacuoles to a semi-autonomous membrane system. Histochem Cell Biol 150, 407–430.
Sato K, Nakano A (2007). Mechanisms of COPII vesicle formation and protein sorting. FEBS Lett 581, 2076–2082.
Stephens DJ, Pepperkok R (2002). Imaging of procollagen transport reveals COPI-dependent cargo sorting during ER-to-Golgi transport in mammalian cells. J Cell Sci 115, 1149–1160.
Suzuki T, Arai S, Takeuchi M, Sakurai C, Ebana H, Higashi T, Hashimoto H, Hatsuzawa K, Wada I (2012). Development of cysteine-free fluorescent proteins for the oxidative environment. PLoS One 7, e37551.
Uversky VN (2017). Intrinsically disordered proteins in overcrowded milieu: membrane-less organelles, phase separation, and intrinsic disorder. Curr Opin Struct Biol 44, 18–30.
Valetti C, Grossi CE, Milstein C, Sitia R (1991). Russell bodies: a general response of secretory cells to synthesis of a mutant immunoglobulin which can neither exit from, nor be degraded in, the endoplasmic reticulum. J Cell Biol 115, 983–994.
Venditti R, Scanu T, Santoro M, Di Tullio G, Spaar A, Gaibisso R, Beznoussenko GV, Mironov AA, Mironov A Jr, Zelante L, *et al.* (2012). Sedlin controls the ER export of procollagen by regulating the Sar1 cycle. Science 337, 1668–1672.
Watson P, Stephens DJ (2005). ER-to-Golgi transport: form and formation of vesicular and tubular carriers. Biochim Biophys Acta 1744, 304–315.
Yu S, Satoh A, Pypaert M, Mullen K, Hay JC, Ferro-Novick S (2006). mBet3p is required for homotypic COPII vesicle tethering in mammalian cells. J Cell Biol 174, 359–368.
Zanetti G, Pahuja KB, Studer S, Shim S, Schekman R (2011). COPII and the regulation of protein sorting in mammals. Nat Cell Biol 14, 20–28.
Zbinden A, Perez-Berlanga M, De Rossi P, Polymenidou M (2020). Phase separation and neurodegenerative diseases: a disturbance in the force. Dev Cell 55, 45–68.
Zhao YG, Zhang H (2020). Phase separation in membrane biology: The interplay between membrane-bound organelles and membraneless condensates. Dev Cell 55, 30–44.